ACADEMIC PRESS

Available online at www.sciencedirect.com
SCIENCE DIRECT®

Journal of Catalysis 217 (2003) 388–395

JOURNAL OF CATALYSIS

www.elsevier.com/locate/jcat

Evaluation of Pt/MCM-41//MgAPO-*n* composite catalysts for isomerization and hydrocracking of *n*-decane

S.P. Elangovan [1] and Martin Hartmann *

University of Kaiserslautern, Department of Chemistry, Chemical Technology, PO Box 3049, D-67653 Kaiserslautern, Germany

Received 7 November 2002; revised 21 January 2003; accepted 21 January 2003

Abstract

The hydroconversion of *n*-decane has been investigated over bifunctional Pt/MCM-41//MgAPO-*n* ($n = 5, 11$) composite catalysts consisting of Pt/MCM-41 as the metal function and different Mg-containing aluminophosphates MgAPO-*n* as the acidic function. Hydrocracking is dominant over the catalysts containing MgAPO-5, while the isomerization selectivity is high over composite catalysts containing MgAPO-11. The higher isomerization selectivity of the latter catalysts is explained in terms of shape selectivity. The acid site density was varied by adding different quantities of MgAPO-*n* to the composite catalyst without changing the overall metal content. The highest selectivity for *n*-decane isomerization is found for a 50/50 physical mixture of 1.0Pt/MCM-41 with MgAPO-11. The distance between the two catalytic functions was varied by mixing of different sized pellets. It was found that the particles with diameters ranging from 1 to ca. 250 μm can be mixed without significant decrease in catalytic activity. The results of this study confirm that the classical bifunctional mechanism for isomerization and hydrocracking of *n*-alkanes is operative under our experimental conditions.

Keywords: *n*-Decane isomerization; MCM-41; MgAPO-5; MgAPO-11; Composite catalysts

1. Introduction

Bifunctional catalyst consisting of metal clusters supported on acidic zeolites are used in various industrial processes, viz. isomerization of C_5/C_6 alkanes, dewaxing, and isomerization of C_8 aromatics. The hydroconversion of *n*-alkanes is achieved over bifunctional catalysts containing highly dispersed noble metal clusters on a support which contains Brønsted acid sites. During the reaction, the noble metal catalyzes hydrogen transfer reactions (hydrogenation–dehydrogenation), while isomerization and hydrocracking occur on the Brønsted acid sites [1]. The well-accepted (classical) reaction mechanism of *n*-decane isomerization proceeds via several steps, viz. (i) dehydrogenation on the noble metal, (ii) protonation of the *n*-alkene on the Brønsted acid site with formation of a secondary alkylcarbenium ion, (iii) rearrangement of the alkylcarbenium ion via formation of cyclic alkylcarbonium-type transition states (PCP mechanism), (iv) deprotonation, and (v) hydrogenation [2]. The importance of *n*-alkane isomerization for improving motor fuel properties, including environmentally benign high-octane gasoline with a limited content of benzene and other aromatics, high-cetane diesel fuel with low pour and cloud points, and high viscosity lubricant base stocks with low pour points is growing. However, the practical application of this process has only been confined to C_4/C_6 alkanes [3–5], because the isomerization of long-chain alkanes is usually accompanied by undesirable cracking. Catalysts with a sufficiently good balance of metal and acid functions under suitable reaction conditions are generally needed to suppress cracking in order to achieve high isomerization selectivity for long-chain alkanes. Platinum and palladium ion-exchanged zeolites are known to give high isomerization yields at medium conversion. However, due to faster cracking of the branched isomers, hydrocracking becomes dominant at high conversion levels. The exact value of the isomerization maximum is expected to be dependent on the balance between the two catalytic functions, viz. the density and the strength of the Brønsted acid sites and the nature, amount, and dispersion of the metal.

Composite catalysts (viz. a physical mixture of two catalyst components) have been used only to a limited extent for alkane isomerization [6–11]. Steinberg et al. [8] reported

* Corresponding author.
E-mail address: hartmann@rhrk.uni-kl.de (M. Hartmann).
[1] On leave from Sri Venkateswara College of Engineering, Pennalur-602 105, Tamil Nadu, India.

0021-9517/03/$ – see front matter
doi:10.1016/S0021-9517(03)00042-3

that the admixture of a protonated zeolite to a Pt/SiO_2 catalyst enhances its *n*-alkane isomerization activity. Assuming that the classical bifunctional mechanism is operative, Weisz [9] already showed in 1962 that the two catalytic functions can be well separated. However, a sufficiently close proximity of metal and acid sites is an important factor for the performance of catalysts in the isomerization of *n*-alkanes. This concept was recently questioned by Fujimoto et al. [10,11] who suggested that hydrogen spillover plays an important role in alkane activation and the stability of intermediates.

Silicoaluminophosphates (SAPOs) have been studied for *n*-alkane isomerization [12–17]. However, most studies focus on the isomerization of C_6 to C_8 *n*-alkanes, while only one paper deals with the isomerization of *n*-decane over Pt/MgAPO-*n* with AEL, AFI, and AFO structures [18]. A new molecular sieve process using Pt/SAPO-11 for lube dewaxing by wax isomerization was described by Miller [19]. Pt/SAPO-11 shows both a high selectivity for wax isomerization and a low selectivity for secondary hydrocracking. Moderate acid activity and the one-dimensional nature of the 10-ring pores appear to contribute to its performance.

In this work, the acid sites of the catalyst have been generated by isomorphous substitution of magnesium into the aluminophosphate framework [18]. In the present study, the behavior of Pt/MCM-41//MgAPO-*n* composite catalysts toward the hydroconversion of *n*-decane is investigated. We have explored the possibility of utilizing MgAPO-5 [AFI (structure code of the International Zeolite Association), $d_p = 0.73$ nm] and MgAPO-11 [AEL, $d_p = 0.63 \times 0.39$ nm] as acid function. The effect of varying metal content on the isomer yield has already been given attention [20]. Here we change the number of acid sites by adding different amounts of MgAPO-*n* to the composite catalyst without changing the overall metal content. The maximum isomer yield is found over the 1.0Pt/MCM-41//MgAPO-11(50/50) catalyst. The formation of multibranched isomers is suppressed over MgAPO-11, which, in turn, reduces the cracking rate, and, hence, results in a higher isomer yield.

The influence of the spatial distance of the two catalytic functions has been studied by mixing (monofunctional) particles with diameters ranging from 1 to 355 μm. It is found that particles with diameters ranging from 1 (powder) to 250 μm can be mixed without a significant decrease in catalytic activity. The results of this study allow the design of novel bifunctional composite catalyst where the two catalytic functions can be tuned separately in order to obtain well-balanced catalysts exhibiting high selectivities for isomerized or cracked products.

2. Experimental

Pure silica MCM-41 was synthesized by dissolving 32 g of tetradecyltrimethylammonium bromide (C_{14}TMABr) in 115 g of water in a polypropylene bottle. Thereafter, 37.4 g of sodium silicate was added dropwise. After 30 min, 2.4 g of concentrated sulfuric acid in 10 g water was added. The gel formed was homogenized by shaking for about 20 min. The resulting gel was kept at 100 °C for about 24 h. MgAPO-5 was synthesized with triethylamine (Et_3N) as the template using the following gel composition: $1.0Al_2O_3$:$1.0P_2O_5$:$0.7Et_3N$:$20.3H_2O$:0.05MgO. The amount of 38.9 g of pseudoboehmite (75 wt%, Condea) was dispersed in 100 g of distilled water for 1 h. Thereafter, 66.6 g of orthophosphoric acid (Merck, 85%) was added dropwise into the mixture and 3.0 g of magnesium acetate (Aldrich, 98%) in 15 g of water was added. After stirring for 1 h, 26.4 g of triethylamine (Fluka, 99.5%) was added. Then the mixture was allowed to stir for 2 h. The resulting gel was crystallized at 200 °C for 36 h. MgAPO-11 was synthesized as follows using a gel composition of $1.0Al_2O_3$:$1.25P_2O_5$:2.37DPA:1.8HF:$156H_2O$:0.05MgO. Aluminum hydroxide (15.5 g, Aldrich) was mixed with 40 g of distilled water and stirred for 1 h. Thereafter, 28.8 g of orthophosphoric acid diluted with 50 g of distilled water was added dropwise. The mixture was again stirred for 1 h followed by the addition of 0.53 g of magnesium acetate in 25 g of water. After 30 min under stirring, 24 g of dipropylamine (DPA) was added and the gel was stirred for another hour. Finally 8.5 g of HF (Riedel-de Haen, 40%) diluted in 20 g of water was added. After 2 h under stirring, the gel was transferred into an autoclave and kept at 145 °C for 18 h. The obtained solid was calcined at 540 °C in a flow of nitrogen for 18 h and subsequently in air for about 4 h. The materials were characterized by X-ray powder diffraction (XRD), nitrogen adsorption, and atomic absorption spectroscopy (AAS). The density and strength of the acid sites of MgAPO-5 and MgAPO-11 were studied by temperature-programmed desorption of pyridine. A 10 mg portion of the calcined material was placed in a quartz reactor and activated overnight in a flow of nitrogen at 350 °C. Thereafter, the material was saturated with pyridine vapor at 50 °C for about 15 min. After purging with nitrogen for 3 h, the temperature was increased to 650 °C at a heating rate of 5 °C/min in a nitrogen flow. The pyridine concentration in the purge flow was analyzed by gas chromatography.

The calcined pure silica MCM-41 materials were repeatedly ion-exchanged with ammonium nitrate at 40 °C. To allow the mixing of different ratios of Pt/MCM-41 and MgAPO-*n* without changing the overall metal content (0.5 wt%), catalysts with different platinum loadings (2.0, 1.0, 0.67, and 0.5 wt%) were prepared employing the impregnation method using $Pt(NH_3)_4Cl_2$ as the precursor. The required amount of metal precursor was dissolved in 50 ml of distilled water and the obtained solution was added dropwise to 1.5 g of the molecular sieve slurred in 50 ml of distilled water. After stirring the resulting solution for 2 h at 40 °C, the water was removed in a rotary evaporator at 60 °C under vacuum. Thereafter, the samples were dried overnight at 100 °C. Finally, the two catalytic components (Pt/MCM-41 and MgAPO-*n*) were physically mixed together in the

powder form, pressed without binder, crushed, and sieved to obtain particles with a diameter of 250 to 355 µm. In one set of experiments, the two catalytic components were pelletized separately and pellets with different sizes were mixed to evaluate the influence of the distance of the two catalytic functions. The catalytic experiments were carried out in a fixed-bed flow-type apparatus with on-line gas chromatographic analysis of the reaction products. The experiments were conducted at a hydrogen pressure of 1 MPa and the pressure of the *n*-decane was adjusted to 10 kPa. The modified residence time $W/F_{n\text{-decane}}$ amounted to 400 g h mol^{-1}. Prior to the catalytic experiments, the catalysts were dehydrated in a flow of argon at 250 °C, calcined in oxygen at 300 °C, then flushed with argon at 400 °C, and finally reduced in hydrogen at 310 °C for 4 h. The conversion was varied by varying the reaction temperature.

3. Results and discussion

The structure and crystallinity of MgAPO-*n* and the structural order of MCM-41 were checked by powder X-ray diffraction (not shown). The textural properties of the employed MCM-41 and MgAPO-*n* materials are summarized in Table 1. The MgAPO-5 and MgAPO-11 microporous molecular sieves possess specific surface areas of 380 and 230 m^2/g, respectively. The n_{Mg}/n_{Al} ratio was determined by AAS to 0.02 and 0.01 for MgAPO-5 and MgAPO-11, respectively. The results show that the AEL structure (MgAPO-11) has a lower tolerance toward the incorporation of magnesium as compared to the AFI structure (MgAPO-5). Similar findings have also been reported in a recent study [21].

The substitution of aluminum by magnesium in the neutral $AlPO_4$-*n* framework creates a negative charge in the framework which is balanced by a bridging proton imparting Brønsted acidity in the MgAPO-*n* samples [22]. The density and the strength of these acid sites has been probed by temperature-programmed desorption of pyridine (Fig. 1). Both samples exhibit a sharp maximum at ca. 150 °C, while for MgAPO-5 a second maximum at 500 °C with a shoulder at 580 °C is observed. The low temperature peak appears at the same position for $AlPO_4$-5 and $AlPO_4$-11 and has been assigned to surface hydroxyls [23]. The high-temperature peak shows a distribution of strong Brønsted acid sites and/or Lewis acid sites. A more detailed characterization

Table 1
Textural properties and chemical composition of the employed catalysts

Catalyst	Specific surface area (m^2/g)	Pore diameter (nm)	n_{Mg}/n_{Al} (AAS)
MgAPO-5	380	0.63 × 0.39	0.02
MgAPO-11	230	0.73	0.01
MCM-41	910	2.8[a]	–

[a] Determined from the nitrogen adsorption isotherm using the BJH method.

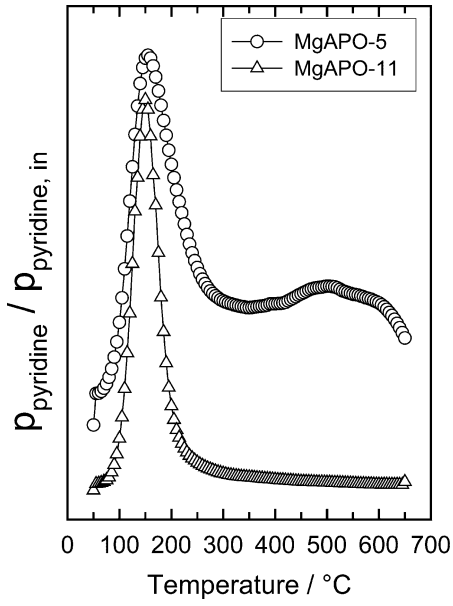

Fig. 1. Temperature-programmed desorption curves of pyridine of MgAPO-5 (○) and MgAPO-11 (△).

of these sites employing IR spectroscopy following pyridine adsorption is currently underway. The apparent absence of a high-temperature peak in MgAPO-11 is probably related to the lower magnesium content of the sample.

Fig. 2 (left) shows the conversion of *n*-decane over bifunctional composite catalysts composed of Pt/MCM-41 as the metal function and MgAPO-5 as the acid function, denoted Pt/MCM-41//MgAPO-5, mixed in different ratios without changing the overall metal content. For comparison, the monofunctional catalysts 0.5Pt/MCM-41 (Pt supported on pure silica MCM-41) and MgAPO-5 are also displayed. In comparison to the monofunctional catalysts, the bifunctional composite catalysts show significantly higher catalytic activity. For the composite catalysts, *n*-decane conversions start at 200 °C and almost complete conversions are reached between 340 and 350 °C. The catalytic activity increases with increasing number of acid sites, viz. with increasing fraction of MgAPO-5 in the composite catalyst. At a reaction temperature of 300 °C, the conversion of *n*-decane over the catalyst 2.0Pt/MCM-41//MgAPO-5(25/75) amounts to 65%, while for 1.0Pt/MCM-41//MgAPO-5(50/50) and 0.67Pt/MCM-41//MgAPO-5(75/25) the conversion reaches ca. 55 and 30%, respectively. Over the monofunctional catalyst Pt/MCM-41, the conversion is below 5%. However, only a low isomer yield ($Y_{iso.} < 10\%$) is found (Fig. 2 (right)), when MgAPO-5 is employed as the acid function. A similar low isomer yield is also observed for 0.5Pt//MgAPO-5, which is ascribed to fast cracking of the formed multibranched isomers [18].

In Fig. 3 (left), the results of *n*-decane conversion over Pt/MCM41//MgAPO-11 composites are depicted. The Pt/MCM-41//MgAPO-11 composites exhibit almost similar catalytic activity compared to composites containing

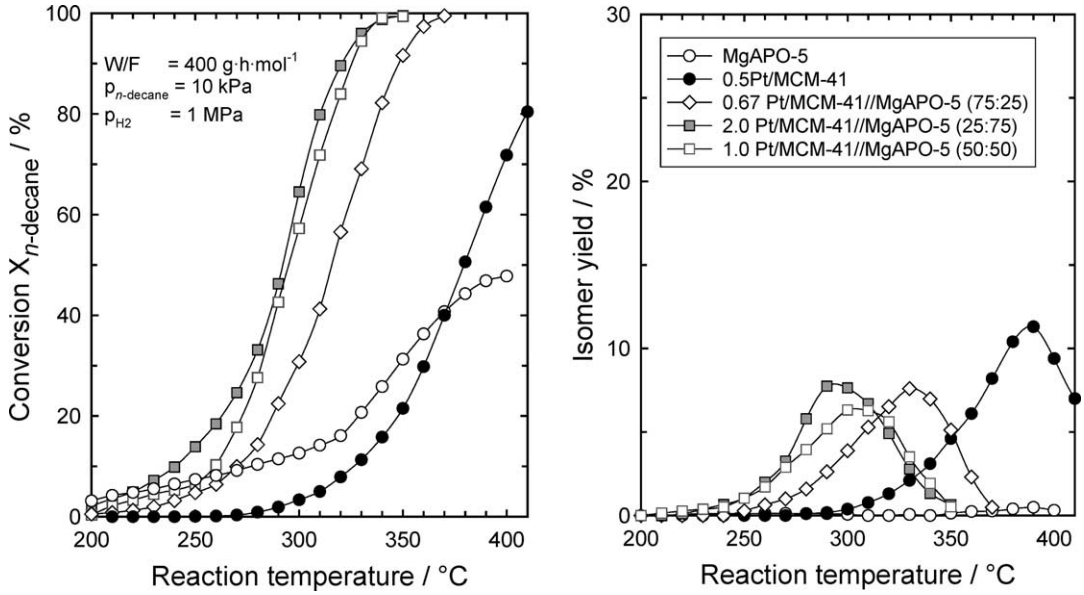

Fig. 2. Conversion of n-decane (left) and isomer yield (right) as a function of the reaction temperature over different Pt/MCM-41//MgAPO-5 composite catalysts. Reaction conditions were $p_{H_2} = 1$ MPa; $p_{n\text{-decane}} = 10$ kPa; $W/F = 400$ g h mol^{-1}.

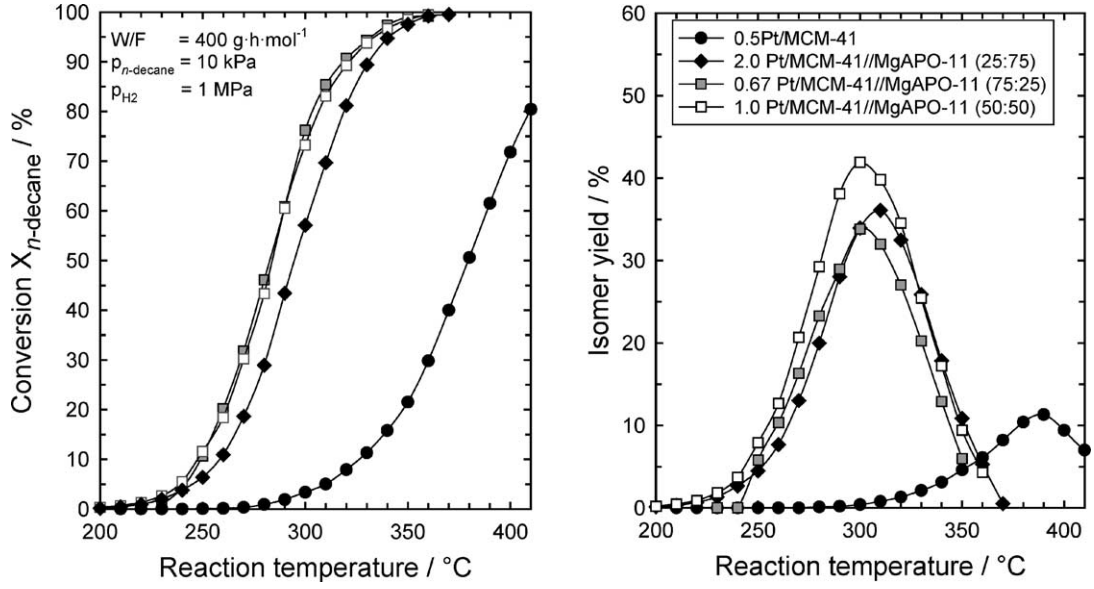

Fig. 3. Conversion of n-decane (left) and isomer yield (right) as a function of the reaction temperature over different Pt/MCM-41//MgAPO-11 composite catalysts. Reaction conditions were $p_{H_2} = 1$ MPa; $p_{n\text{-decane}} = 10$ kPa; $W/F = 400$ g h mol^{-1}.

MgAPO-5, but a significantly higher isomer yield of above 35% (Fig. 3 (right)) is observed. The experimental results are in complete agreement with the well-known reaction mechanism for isomerization and hydrocracking of n-alkanes [24]. With increasing conversion, the isomer yield passes through a maximum, indicating that the branched hydrocarbons are consumed by hydrocracking. In essence, the n-decane feed is isomerized (i.e., branching is created) until a configuration is reached at which hydrocracking (i.e., cleavage of carbon–carbon bonds, so called ionic β-scission) occurs.

The isomer distribution over Pt/MCM-41//MgAPO-n mixed in equal amounts (50/50) is depicted in Fig. 4 as a function of n-decane conversion. At low conversion, monobranched isomers are formed exclusively. With increasing overall conversion, the content of dibranched isomers increases monotonically at the expense of the monobranched isomers. In principle, the consecutive formation of an increasing number of branching in the feed molecule is in agreement with the proposed reaction mechanism. Over 1.0Pt/MCM-41//MgAPO-5(50/50), a low selectivity for dibranched isomers is observed, while tribranched isomers are practically not formed. This is attributed to the fast hydrocracking of the di- and tribranched isomers over MgAPO-5. The 1.0Pt/MCM-41//MgAPO-

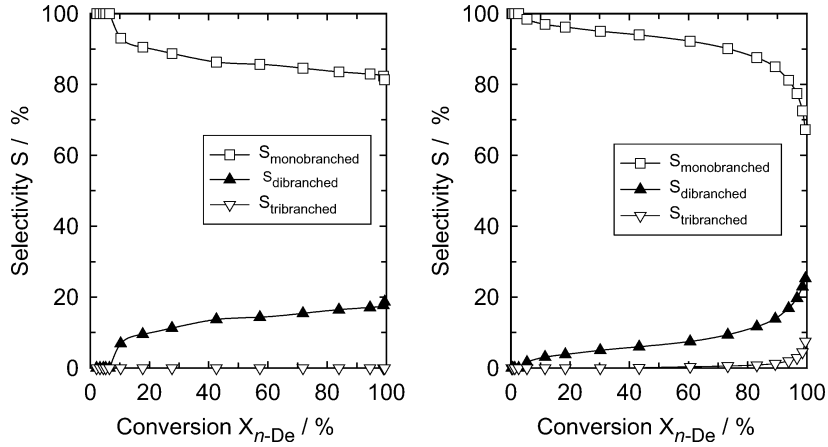

Fig. 4. Isomer distribution over 1.0Pt/MCM-41//MgAPO-5(50/50) (left) and Pt/MCM-41//MgAPO-11(50/50) (right) as a function of conversion of *n*-decane.

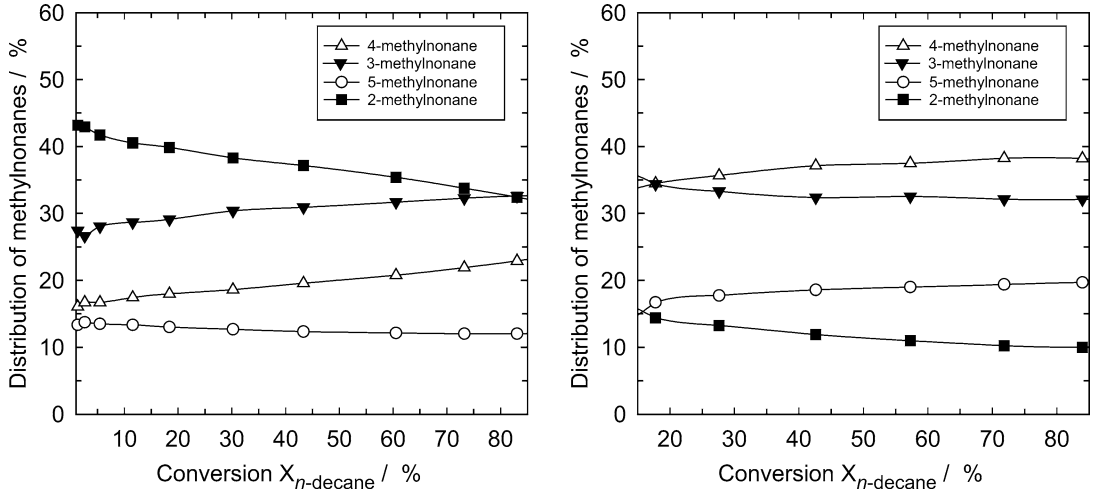

Fig. 5. Distribution of methylnonanes over 1.0Pt/MCM-41//MgAPO-11(50/50) (left) and Pt/MCM-41//MgAPO-5(50/50) (right) as a function of conversion of *n*-decane.

11(50/50) composite catalyst exhibits an even lower selectivity to multibranched isomers. A similar behavior has also been found for 0.5Pt/MgAPO-11 and ascribed to the hindered formation of multiply branched isomers in the 10-membered ring channels of MgAPO-11 [18]. In addition, it could be assumed that the diffusion of the monobranched isomers out of the narrow pores of the molecular sieves is faster than the diffusion of the more bulky di- or tribranched isomers. Similar results are observed with the composite catalysts having a lower or higher number of acid sites, viz. 0.67Pt/MCM-41//MgAPO-11(75/25) and 2.0Pt/MCM-41//MgAPO-11(25/75).

Fig. 5 shows the distribution of the methylnonanes as a function of *n*-decane conversion over the 1.0Pt/MCM-41//MgAPO-11(50/50) catalyst and the 1.0Pt/MCM-41//MgAPO-5(50/50) catalyst, where the relative distribution of methylnonanes approaches thermodynamic equilibrium at high conversion (Fig. 5 (right)). Assuming that the formation of the methylnonanes proceeds over protonated cyclopropanes (PCP mechanism), the theoretical distribution of methylnonanes is 33.3% 3-methylnonane, 33.3% 4-methylnonane, 16.7% 2-methylnonane, and 16.7% 5-methylnonane [25]. In contrast to the theoretical distribution, only a low yield of 4-methylnonane is observed experimentally over 1.0Pt/MCM-41//MgAPO-11(50/50) (Fig. 5 (left)). This is probably due to the restricted formation of the 4-methyl non-5 cation in the 10-membered ring channels of MgAPO-11, which leads to the formation of 4-methylnonane. Bifunctional catalysts based on other 10-membered ring molecular sieves, viz. ZSM-5, ZSM-11, and ZSM-22, also exhibit a similar molecular shape selectivity in the conversion of *n*-decane [26,27]. A typical feature of 10-membered ring zeolites is the suppressed formation of di- and tribranched isomers and the decreased rate of 4-methylnonane and 5-methylnonane formation as compared to 2-methyl branching due to steric constraints. Moreover, it has been found that only minor amounts of dibranched isomers desorb from 10-membered ring zeolites such as ZSM-5 [28]. Based on the relative distribution of methylnonanes, a refined constraint index CI° was defined as the yield ratio of

Table 2
Distribution of the cracked products at a cracking yield Y_{Cr} of 15%

Catalyst	Number of moles/100 mol cracked					
	2.0Pt/MCM-41// MgAPO-5(25/75)	1.0Pt/MCM-41// MgAPO-5(50/50)	0.67Pt/MCM-41 MgAPO-5(75/25)	2.0Pt/MCM-41// MgAPO-11(25/75)	1.0Pt/MCM-41// MgAPO-11(50/50)	0.67Pt/MCM-41// MgAPO-11(75/25)
C_1	0	3	7	21	15	11
C_2	0	2	5	6	7	8
$C_3 + C_7$	9	33	50	52	57	62
$C_4 + C_6$	106	102	90	84	76	75
C_5	84	65	52	46	39	39
C_8	0	1	4	4	5	5
C_9	0	1	1	4	7	6
Total	199	207	209	217	216	206
			% iso			
C_4	79.9	66.8	48.2	27.5	10.9	6.5
C_5	86.8	75.3	48.7	31.8	14.5	8.7

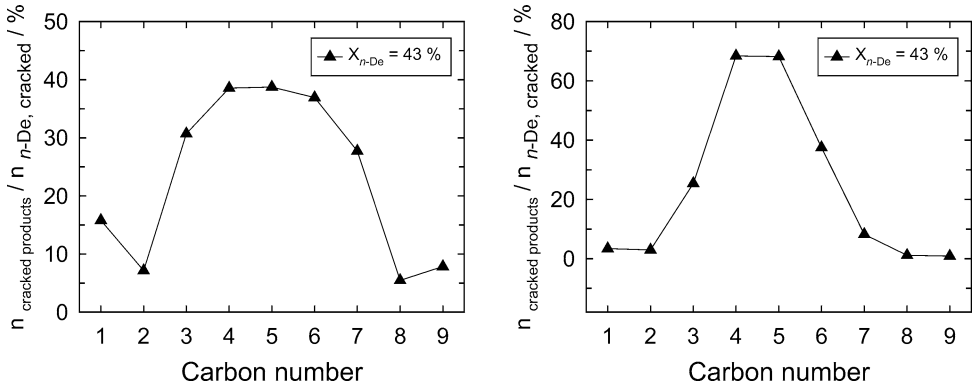

Fig. 6. Distribution of the cracked products over 1.0Pt/MCM-41//MgAPO-11(50/50) (left) and 1.0Pt/MCM-41//MgAPO-5(50/50) (right).

2-methylnonane to 5-methylnonane at 5% isomer yield. The refined constraint index for the 1.0Pt/MCM-41//MgAPO-11(50/50) composite catalyst is found to be 3.8. This is in agreement with the CI° observed for other 10-membered ring molecular sieves such as ZSM-5 (CI° = 4.5), ZSM-11 (2.8), ZSM-22 (>14) [29,30], and MgAPO-11 (3.6) [18] and confirms that the isomerization takes place in the channels of MgAPO-11 in the Pt/MCM-41//MgAPO-11 composite catalysts.

Table 2 summarizes the cracked product distribution expressed in moles of cracked products formed per 100 mol of *n*-decane. The distribution of the cracked products, in particular the absence of methane and ethane, is indicative of ideal hydrocracking with an ionic mechanism of cleavage. Pure primary cracking occurs when the number of moles formed from 100 mol feed does not exceed 200 [25]. In particular, over Pt/MCM-41//MgAPO-5 composites the formation of methane and ethane is observed only to a small extent, which shows that hydrogenolysis on the platinum clusters plays only a minor role. However, the higher amount of C_3 and C_4 alkanes in the product compared to C_6 and C_7 alkanes indicates that the formed alkanes undergo further cracking to yield C_3 and C_4 alkanes (secondary cracking) (Fig. 6). Secondary cracking is often observed over catalysts without well-balanced acid and metal functions. Over Pt/MCM-41//MgAPO-11 composite catalysts, the distribution of cracked products is distinctly different (Fig. 6 (left)). A higher fraction of C_3 and C_7 alkanes is formed so that no clear maximum of the cracked product distribution is observed. Weitkamp et al. [28] reported an analogous distribution over Pt/ZSM-5, which also possesses 10-membered ring channels. The slightly higher amount of methane formation as compared to systems containing MgAPO-5 is attributed to hydrogenolysis.

Table 2 also depicts the amount of branched isomers in the C_4 and C_5 fraction as a function of *n*-decane conversion over the composite catalysts employed in the present study. For composites containing MgAPO-5, the C_4 and C_5 products are mainly branched and their relative amount changes only slightly with the degree of conversion. In contrast, over MgAPO-11 composites mainly *n*-isomers are formed at low conversion levels, while the formation of branched isomers increases with conversion. The observed high selectivities for linear cracking products probably involves hydrocracking of methylnonanes via type C β-scission [28]. Cracking of monobranched alkenes proceeds through a type C mechanism (which involves two secondary carbenium ion intermediates) and results in the formation of two linear alkanes. Dibranched alkenes undergo cracking through type B1 or B2 mechanisms (one secondary and one

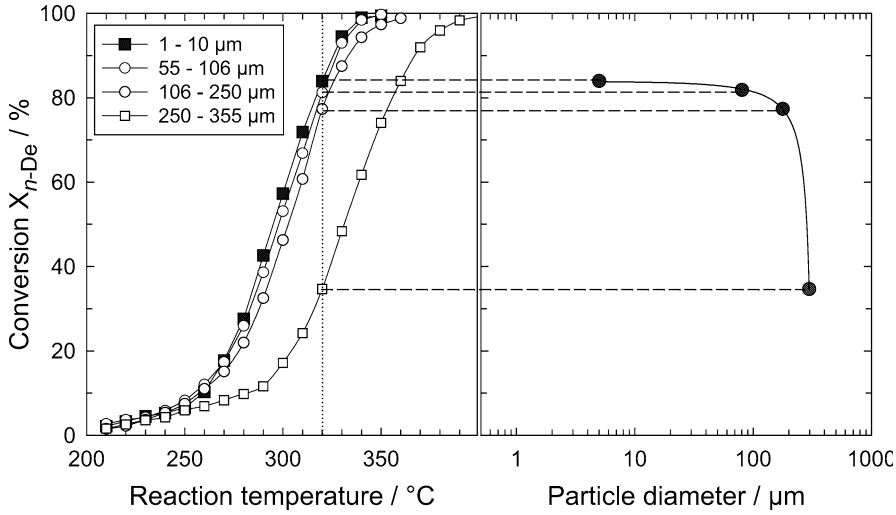

Fig. 7. Conversion of *n*-decane over 1.0Pt/MCM-41//MgAPO-5(50/50) catalyst as a function of particle diameter.

tertiary carbenium ion) and equimolar amounts of branched and linear products are formed. Finally, tribranched alkenes are cracked via type A β-scission (two tertiary carbenium ions) and result in the formation of branched isomers. Type D β-scission via primary carbenium ions is typically not observed over zeolites. Type A cracking is much faster than type B which is again faster than type C cracking. Therefore, over MgAPO-5 composite catalysts the cracked products are predominantly formed via type A β-scission, which accounts for the high selectivities for branched isomers [31]. However, over mixtures containing MgAPO-11 lower selectivities for branched isomers may be attributed to contributions from type B (B1 and B2) and type C cracking mechanism.

In order to avoid that the reaction rate is limited by alkene transport, the two catalytic functions need to be at sufficiently short mutual distances (intimacy criterion). The intimacy criterion has been proposed by Weisz in 1962 [9]:

$$R_c^2 \leqslant 1.2 \times 10^5 \frac{p_0 D_0}{T \cdot \mathrm{d}N/\mathrm{d}t}. \quad (1)$$

In this expression, p_0 (in MPa) and D_0 (in $\mathrm{m^2\,s^{-1}}$) denote the partial pressure and the diffusion coefficient of the intermediate alkene, respectively. T (in K) is the reaction temperature, R_c (in m) is the radius of the catalyst particles (which is a measure for the spatial separation of the two functions) and $\mathrm{d}N/\mathrm{d}t$ (in $\mathrm{mol\,s^{-1}\,m^{-3}}$) is the intrinsic reaction rate of the acid-catalyzed alkene conversion. The realization of sufficient intimacy in a composite catalyst is critical because of the slow micropore diffusion of the hydrocarbons and the high catalytic turnover numbers of the acid sites [32]. In this context, we have explored the possibility of varying the distance between the two catalytic functions by changing the particle radius of two different catalyst particles in a series of experiments. Fig. 7 shows the conversion of *n*-decane over Pt/MCM-41//MgAPO-5(50/50) composite catalysts, where particles with different particle sizes have been mixed. With increasing particles size from ca. 1 µm (i.e., the Pt/MCM-41 and MgAPO-5 powders are mixed) to ca. 106 to 250 µm, *n*-decane conversion is decreasing only slightly, which confirms that the two catalytic functions are in sufficient intimacy. The observed product mixture exclusively consists of *n*-decane isomers and cracked products. The formation of *n*-decene or other olefins is *not* observed. Further increase of the particle size to ca. 250 to 355 µm results in a sharp decline of *n*-decane conversion, which shows that the two catalytic functions are too far apart under the prevailing reaction conditions. A similar decline of catalytic activity with particle size is observed for Pt/MCM-41//MgAPO-11(50/50) composite catalysts (Fig. 8). In addition, the complete absence of olefins in the product suggests that the reaction proceeds over the classical bifunctional mechanism exclusively yielding isomerization and cracking products. The results presented here also confirm that the two catalytic functions can be well separated (ca. 200 µm) in *n*-decane conversion over bifunctional catalysts based on Pt/MCM-41 and MgAPO-*n*. This allows using different supports for the acid and metal function, respectively, without significant decrease in catalytic activity. Moreover, in the light of the recent criticism of the classical

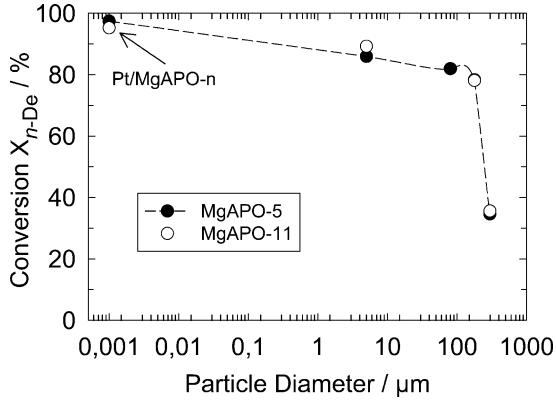

Fig. 8. Conversion of *n*-decane over 1.0Pt/MCM-41//MgAPO-11(50/50) catalyst as a function of particle diameter.

bifunctional mechanism [10,11,33,34] our work is reminiscent of the earlier work of Weisz [9], who studied mixtures of Pt/SiO_2 and silica–alumina. Their observation that the mixture was much more reactive for *n*-hexane isomerization than each of the individual components supported the concept of a bifunctional catalyst, and, hence, the results were interpreted according to the classical mechanism. As a result of diffusional limitations, the extent of conversion is determined by the distance (i.e., particle size) of the two catalytic functions. This is clearly confirmed in the present study. Therefore, the model of Iglesia et al. [34], which requires that the two catalytic functions are adjacent to each other, is not valid under our conditions. The concept of hydrogen spillover as proposed by Fujimoto and co-workers [10,11] requires the transfer of hydrogen atoms or ions from one catalyst particle to another. The mechanism by which hydrogen spillover between catalyst particles could occur is not obvious and it seems better to seek alternative explanations.

The influence of separating metal and acid sites on their proposed reaction mechanism was also considered by Chu et al. [33]. They concluded that the cracking selectivity at a fixed temperature will decrease with increasing distance of the two catalytic functions. However, in our experiments, the isomerization selectivity at a given temperature does not decline with increasing distance between the two catalytic functions. We, therefore, believe that the classical bifunctional mechanism is still valid under our experimental conditions provided that we use a longer *n*-alkane such as decane and operate at elevated temperatures between 250 and 320 °C.

4. Conclusions

The hydroconversion of *n*-decane has been studied over bifunctional composite catalysts containing Pt/MCM-41 as the metal function and a microporous aluminophosphate MgAPO-5 and MgAPO-11, respectively, as the acid function. Particles with diameters ranging from 1 to 250 μm can be mixed without a significant decrease in catalytic activity. It follows from these studies that the two catalytic functions can be tuned separately to obtain well-balanced catalysts in order to achieve high selectivities for isomerized or cracked products. The use of the 12-membered ring aluminophosphate MgAPO-5 ($d_p = 0.73$ nm) results in isomer yields below 10%, while with MgAPO-11 (10-membered ring pore opening with a pore diameter of 0.39×0.63 nm) a maximum isomer yield of ca. 45% is achieved at a reaction temperature of 300 °C. Over MgAPO-11, the formation of dibranched isomers is suppressed, which results in a reduced cracking rate and, hence, in a higher isomer yield.

Acknowledgment

Financial support of this work by Fonds der Chemischen Industrie is gratefully acknowledged.

References

[1] M.L. Coonradt, W.E. Garwood, Ind. Eng. Chem. Prod. Res. Dev. 3 (1964) 38.
[2] J.A. Martens, M. Tielen, P.A. Jacobs, J. Weitkamp, Zeolites 4 (1984) 98.
[3] S.T. Sie, in: G. Ertl, H. Knoezinger, J. Weitkamp (Eds.), Handbook of Heterogeneous Catalysis, VCH/Wiley, New York, 1997, p. 1998.
[4] P.J. Kuchar, J.C. Bricker, M.E. Reno, R.S. Haizmann, Fuel Process. Technol. 35 (1993) 183.
[5] M.A. Lanewala, P.E. Pickert, A.P. Bolton, J. Catal. 9 (1967) 95.
[6] R. Parton, L. Uytterhoeven, J.A. Martens, P.A. Jacobs, G.F. Froment, Appl. Catal. 76 (1991) 131.
[7] G. Kinger, D. Majda, H. Vinek, Appl. Catal. 225 (2002) 301.
[8] K.H. Steinberg, U. Mroczek, F. Roessner, in: K.H. Steinberg (Ed.), Proc. 2nd International Conference on Spillover, Karl Marx University, Leipzig, 1989, pp. 150–166.
[9] P.B. Weisz, Adv. Catal. 13 (1962) 137.
[10] K. Fujimoto, K. Maeda, K. Aimoto, Appl. Catal. 91 (1992) 81.
[11] T. Kusakari, K. Tomishige, K. Fujimoto, Appl. Catal. 224 (2002) 219.
[12] B. Parlitz, E. Schreier, H.-L. Zubowa, R. Eckelt, E. Lieske, G. Lischke, R. Fricke, J. Catal. 155 (1995) 1.
[13] A. Chica, A. Corma, J. Catal. 187 (1999) 167.
[14] P. Meriaudeau, V.A. Tuan, V.T. Nghiem, S.Y. Lai, L.N. Hung, C. Naccache, J. Catal. 169 (1997) 55.
[15] M. Hoechtl, A. Jentys, H. Vinek, Micropor. Mesopor. Mater. 31 (1999) 271.
[16] P. Meriaudeau, V.A. Tuan, V.T. Nghiem, G. Sapaly, C. Naccache, J. Catal. 185 (1999) 435.
[17] J.M. Campelo, F. Lafont, J.M. Marinas, Appl. Catal. 152 (1997) 53.
[18] M. Hartmann, S.P. Elangovan, Chem. Ing. Tech. 74 (2002) 1262.
[19] S.J. Miller, Micropor. Mater. 2 (1994) 439.
[20] F. Alvarez, F.R. Ribeiro, G. Perot, C. Thomazeau, M. Guisnet, J. Catal. 162 (1996) 179.
[21] R. Fernandez, M.V. Giotto, H.O. Pastare, D. Cardoso, Micropor. Mesopor. Mater. 53 (2002) 135.
[22] S. Prasad, D.H. Barich, J.F. Haw, Catal. Lett. 39 (1996) 141.
[23] J. Das, V.V. Satyanarayana, D.K. Chakraborthy, S.N. Piramanayagam, S.N. Shrinji, J. Chem. Soc., Faraday Trans. 88 (1992) 3255.
[24] J. Weitkamp, Ind. Eng. Chem. Prod. Res. Dev. 21 (1982) 550.
[25] J.A. Martens, P.A. Jacobs, Zeolites 6 (1986) 334.
[26] P.A. Jacobs, J.A. Martens, J. Weitkamp, H.K. Beyer, Faraday Discuss. Chem. Soc. 72 (1982) 353.
[27] J.A. Martens, R. Parton, L. Uytterhoeven, P.A. Jacobs, G.F. Froment, Appl. Catal. 76 (1991) 95.
[28] J. Weitkamp, P.A. Jacobs, J.A. Martens, Appl. Catal. 8 (1983) 123.
[29] S. Ernst, J. Weitkamp, J.A. Martens, P.A. Jacobs, Appl. Catal. 48 (1989) 137.
[30] J. Weitkamp, S. Ernst, Catal. Today 19 (1994) 107.
[31] J.A. Martens, P.A. Jacobs, J. Weitkamp, Appl. Catal. 20 (1986) 283.
[32] P.A. Jacobs, J.A. Martens, Stud. Surf. Sci. Catal. 58 (1991) 445.
[33] H.Y. Chu, M.P. Rosynek, J.H. Lunsford, J. Catal. 178 (1998) 352.
[34] E. Iglesia, S.L. Soled, G.M. Kramer, J. Catal. 144 (1993) 238.